Two-loop QED corrections with closed fermion loops

V. A. Yerokhin,[1] P. Indelicato,[2] and V. M. Shabaev[3]

[1]*Center for Advanced Studies, St. Petersburg State Polytechnical University, Polytekhnicheskaya 29, St. Petersburg 195251, Russia*

[2]*Laboratoire Kastler-Brossel, École Normale Supérieure, CNRS et Université P. et M. Curie, Case 74, 4 pl. Jussieu, F-75252, France*

[3]*Department of Physics, St. Petersburg State University, Oulianovskaya 1, St. Petersburg 198504, Russia*

We report a calculation of all two-loop QED corrections with closed fermion loops for the $n = 1$ and $n = 2$ states of H-like ions and for a wide range of the nuclear charge numbers $Z = 1-100$. The calculation is performed to all orders in the binding-strength parameter $Z\alpha$, with the exception that in a few cases the free-loop approximation is employed in the treatment of the fermion loops. Detailed comparison is made with previous $Z\alpha$-expansion calculations and the higher-order remainder term to order $\alpha^2(Z\alpha)^6$ is identified.

PACS numbers: 31.30.jf, 31.15.A-, 31.10.+z

Introduction

Highly charged ions are often considered as the ideal testing ground for investigating the strong-field regime of bound-state quantum electrodynamics (QED). They feature a strong static Coulomb field of the nucleus and have a simple electronic structure, which can be accurately determined in *ab initio* theoretical calculations. In this respect, the ultimate investigation object is the H-like uranium, the heaviest naturally occurring element. Measurements of the $1s$ Lamb shift in H-like uranium have progressed drastically during last decades [1, 2], having achieved an accuracy of 4.6 eV [3], which corresponds to a fractional error of 1.7% with respect to the total QED contribution. Further advance anticipated in the future will make such experiments sensitive to the two-loop QED effects.

Even higher precision is achieved for heavy Li-like ions. Measurements of the $2p_{1/2,3/2}$-$2s$ transition energies [4, 5, 6, 7, 8] have lately reached a fractional accuracy of 0.03% with respect to the total QED contribution. This corresponds to a 10% sensitivity of the experimental results to the two-loop QED effects. These measurements provide an excellent possibility for the identification of the two-loop Lamb shift and for testing the bound-state QED up to second order in α in the strong-field regime (α is the fine-structure constant). Theoretical description of Li-like ions is more complicated than that of H-like ions, which is due to the presence of additional electrons. For heavy systems, the electron-electron interaction is weak (as compared to the electron-nucleus interaction) and can be successfully treated by perturbation theory. *Ab initio* calculational results for the effects of the electron correlation and the screening of one-loop QED corrections are already available for Li-like ions [9, 10]; their accuracy is sufficient for identification of the two-loop QED effects.

The detailed theoretical understanding of the two-loop QED effects is also necessary for the interpretation of high-precision experimental data in the low-Z region. The most prominent example here is hydrogen. Its spectroscopy can nowadays be realized with a relative accuracy on the level of 10^{-14} [11, 12]. The theoretical understanding of the $1s$ and $2s$ Lamb shift in hydrogen is still limited, to a large extent, by the two-loop QED effects [13].

The subject of our present interest is the set of the two-loop QED corrections (also referred to as the two-loop Lamb shift), graphically represented in Fig. 1. These corrections have been intensively investigated within the perturbative expansion in the binding-strength parameter $Z\alpha$ [14, 15, 16, 17] (Z is the nuclear charge number). The results of these studies, however, do not provide reliable information about the magnitude of the two-loop Lamb shift in heavy ions, where the parameter $Z\alpha$ approaches unity. A non-perturbative (in $Z\alpha$) evaluation of the whole set of the two-loop diagrams is needed for the interpretation of experimental results available in the middle- and high-Z region.

Numerical all-order calculations of the two-loop corrections started in late 1980s [18, 19, 20, 21, 22, 23] and dealt with the diagrams with the closed fermion loops [Fig. 1(d)-(k)]. An evaluation of the three remaining diagrams [Fig. 1(a)-(c)], referred to as the two-loop self-energy diagrams, turned out to require considerable efforts. It was accomplished in a series of investigations [24, 25, 26, 27, 28, 29, 30, 31] for the nuclear charge numbers $Z \geq 10$ for the ground state and $Z \geq 60$ for the $n = 2$ states.

The goal of this work is to perform a detailed investigation of all two-loop diagrams with the closed fermion loops [Fig. 1(d)-(k)], extending previous evaluations to cover the whole region of the nuclear charge numbers $Z = 1 - 100$ and all $n = 1$ and $n = 2$ states. The first results of our calculation were presented in Ref. [31]. At present, our intention is to achieve high numerical accuracy in the low-Z region. This will allow us to make a detailed comparison with the perturbative calculations and to isolate the non-perturbative remainder to order $\alpha^2(Z\alpha)^6$, which is of experimental interest for hydrogen. Our calculation will be performed to all orders in the binding-strength parameter $Z\alpha$, but an approximation

will be made in the treatment of the fermion loops in the diagrams in Fig. 1(h)-(k). This approximation, referred to as the *free-loop* one, consists in keeping the leading nonvanishing term of the expansion of the fermion loop in terms of the binding potential. In the one-loop case, it corresponds to the Uehling potential and yields the dominant contribution even for high-Z ions. To perform a non-perturbative calculation of the diagrams in Fig. 1(h)-(k) without the free-loop approximation is a difficult and a so far unsolved problem.

The paper is organized as follows. In Section I, we describe our approach to the evaluation of the one-loop self-energy and vacuum-polarization corrections, which is used as a basis for treatment of the two-loop corrections. In Section II, we discuss the evaluation of individual two-loop corrections with closed fermion loops, present our numerical results, and compare them with the data obtained within the perturbative $Z\alpha$-expansion approach. In Section III, we summarize our results.

The relativistic units ($\hbar = c = 1$) are used in this paper.

I. ONE-LOOP QED CORRECTIONS

We start with presenting some basic formulas for the first-order self-energy and vacuum-polarization corrections that will be needed below in addressing the two-loop corrections.

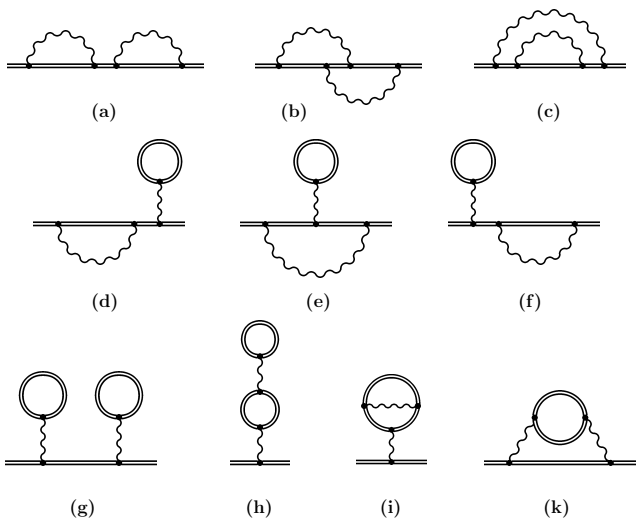

FIG. 1: Two-loop one-electron QED corrections. Gauge-invariant subsets are referred to as SESE (a-c), SEVP (d-f), VPVP (g-i), and S(VP)E (k).

A. Self-energy

The one-loop self-energy (SE) correction to the Lamb shift can be represented as a matrix element of the renormalized SE operator Σ_R,

$$\Delta E_{\rm SE} = \langle a|\gamma^0 \Sigma_R(\varepsilon_a)|a\rangle\,, \tag{1}$$

where $\Sigma_R = \Sigma - \delta m$, δm is the one-loop mass counterterm, ε_a is the energy of the reference state, Σ is the unrenormalized SE operator,

$$\begin{aligned}\Sigma(\varepsilon, \boldsymbol{x}_1, \boldsymbol{x}_2) \;=\; & 2i\alpha\gamma^0 \int_{-\infty}^{\infty} d\omega\, \alpha_\mu \\ & \times G(\varepsilon-\omega, \boldsymbol{x}_1, \boldsymbol{x}_2)\, \alpha_\nu\, D^{\mu\nu}(\omega, \boldsymbol{x}_{12})\;,\end{aligned} \tag{2}$$

G is the Dirac Coulomb Green function $G(\varepsilon) = [\varepsilon - \mathcal{H}(1-i0)]^{-1}$, $\mathcal{H}$ is the Dirac Coulomb Hamiltonian, $D^{\mu\nu}$ is the photon propagator, $\alpha^\mu = (1, \boldsymbol{\alpha})$, and $\boldsymbol{x}_{12} = \boldsymbol{x}_1 - \boldsymbol{x}_2$. It is assumed that the above expressions are regularized in a covariant way and that the limit that removes the regularization is properly approached.

In order to facilitate the numerical evaluation of the above expressions, one needs to explicitly eliminate divergences from the SE operator. A popular method of doing this [32] is based on the expansion of the SE operator in terms the binding field,

$$\Sigma = \Sigma^{(0)} + \Sigma^{(1)} + \Sigma^{(2+)}\,, \tag{3}$$

where the superscript (i), $i = 0, 1$ indicates the total number of interactions with the binding Coulomb field and the index $(2+)$ labels the term generated by ≥ 2 such interactions. Only the first two terms of the expansion are divergent; all divergences can be shown to vanish in the difference $\Sigma - \delta m$. The divergent parts are regularized by working in an extended number of dimensions and evaluated in momentum space, see Ref. [33] for details. We mention that the first-order expansion term $\Sigma^{(1)}$ is usually represented as a product of the time component of the standard vertex operator $\Gamma^\alpha(p_1, p_2)$ and the Coulomb potential V_C,

$$\Sigma^{(1)}(p_1, p_2) \equiv \Gamma^0(p_1, p_2)\, V_C(|\boldsymbol{p_1} - \boldsymbol{p_2}|)\,. \tag{4}$$

The energy shifts induced by (the final parts of) the three terms in the right-hand-side of Eq. (3) are referred to as the zero-, one-, and many-potential terms, respectively:

$$\Delta E_{\rm SE} = \Delta E^{(0)}_{\rm SE} + \Delta E^{(1)}_{\rm SE} + \Delta E^{(2+)}_{\rm SE}\;, \tag{5}$$

where

$$\Delta E^{(0)}_{\rm SE} = \int \frac{d\boldsymbol{p}}{(2\pi)^3}\, \overline{\psi}_a(\boldsymbol{p})\, \Sigma^{(0)}_R(p)\, \psi_a(\boldsymbol{p})\,, \tag{6}$$

$$\Delta E^{(1)}_{\rm SE} = \int \frac{d\boldsymbol{p}_1 d\boldsymbol{p}_2}{(2\pi)^6}\, \overline{\psi}_a(\boldsymbol{p}_1)\, \Gamma^0_R(p_1, p_2)\, V_C(\boldsymbol{q})\, \psi_a(\boldsymbol{p}_2)\,, \tag{7}$$

$$\Delta E^{(2+)}_{\rm SE} = \int d\boldsymbol{x}_1 d\boldsymbol{x}_2\, \overline{\psi}_a(\boldsymbol{x}_1)\, \Sigma^{(2+)}(\varepsilon_a, \boldsymbol{x}_1, \boldsymbol{x}_2)\, \psi_a(\boldsymbol{x}_2)\,, \tag{8}$$

where $\boldsymbol{q} = \boldsymbol{p}_1 - \boldsymbol{p}_2$, $\overline{\psi}_a = \psi_a^\dagger \gamma^0$, $V_C(\boldsymbol{q}) = -4\pi Z\alpha/|\boldsymbol{q}|^2$ is the Coulomb potential in momentum space, $\Sigma^{(0)}_R(p)$ is the finite part of the subtracted free SE operator $\Sigma^{(0)}(p) - \delta m$, $\Gamma^\mu_R(p_1, p_2)$ is the finite part of the vertex operator $\Gamma^\mu(p_1, p_2)$; and p, p_1, and p_2 are four-vectors with the time component fixed by $p^0 = p_1^0 = p_2^0 = \varepsilon_a$. The operator $\Sigma^{(2+)}$ is obtained from Eq. (2) by the substitution $G \to G^{(2+)}$, where the index (2+) denotes, as usual, two or more interactions with the binding Coulomb field.

In the extended number of dimensions, $D = 4 - 2\epsilon$, the free SE operator $\Sigma^{(0)}$ is given by

$$\Sigma^{(0)}(p) = -4\pi i\alpha\mu^{2\epsilon} \int \frac{d^D k}{(2\pi)^D}\, \frac{1}{k^2}\, \frac{\gamma_\sigma(\not{p} - \not{k} + m)\gamma^\sigma}{(p-k)^2 - m^2}\,, \tag{9}$$

where $\not{p} = p^\nu \gamma_\nu$ and μ is the auxiliary mass parameter introduced in order to keep the proper dimension of the interaction term in the Lagrangian. The momentum integration in Eq. (9) is simple; it is described, e.g., in Appendix A of Ref. [28]. Omitting terms of order ϵ and higher, one obtains

$$\begin{aligned}\Sigma^{(0)}(p) - \delta m \;=\; & -\frac{\alpha C_\epsilon}{4\pi\epsilon}(\not{p} - m) \\ & + \frac{\alpha}{4\pi}\left[2m\left(1 + \frac{2\rho}{1-\rho}\ln\rho\right)\right. \\ & \left. - \not{p}\,\frac{2-\rho}{1-\rho}\left(1 + \frac{\rho}{1-\rho}\ln\rho\right)\right], \end{aligned} \tag{10}$$

where $\rho = (m^2 - p^2)/m^2$ and $C_\epsilon = \Gamma(1+\epsilon)(4\pi)^\epsilon \left(\mu^2/m^2\right)^\epsilon$. The operator $\Sigma^{(0)}_R$ in Eq. (6) is the finite part of the right-hand-side of Eq. (10) when ϵ approaches zero.

The free vertex operator Γ^α is

$$\begin{aligned}\Gamma^\alpha(p_1, p_2) \;=\; & -4\pi i\alpha\mu^{2\epsilon} \int \frac{d^D k}{(2\pi)^D}\, \frac{1}{k^2}\gamma_\sigma \frac{\not{p}_1 - \not{k} + m}{(p_1 - k)^2 - m^2} \\ & \times\gamma^\alpha \frac{\not{p}_2 - \not{k} + m}{(p_2 - k)^2 - m^2}\gamma^\sigma\,. \end{aligned} \tag{11}$$

The momentum integration is performed by using the standard technique (see, e.g., Appendix A of Ref. [28]). Omitting terms of order ϵ and higher, one obtains

$$\begin{aligned}\Gamma^\alpha(p_1, p_2) \;=\; & \frac{\alpha C_\epsilon}{4\pi\epsilon}\,\gamma^\alpha - \frac{\alpha}{4\pi}\left[\frac{3}{2}\gamma^\alpha\right. \\ & \left. + \int_0^1 dx dy\, \left(\frac{N^\alpha(xb)}{D} + 2x\gamma^\alpha \ln D\right)\right], \end{aligned} \tag{12}$$

where $N^\alpha(xb) = \gamma_\sigma(\not{p}_1 - x\not{b} + m)\gamma^\alpha(\not{p}_2 - x\not{b} + m)\gamma^\sigma$, $b = yp_1 + (1-y)p_2$, and $D = xb^2 + m^2 - yp_1^2 - (1-y)p_2^2$. The operator Γ^α_R in Eq. (6) is the finite part of the right-hand-side of Eq. (12) when ϵ approaches zero.

Out of the three terms in Eq. (5), the third one $[\Delta E^{(2+)}_{\rm SE}]$ is the most difficult to evaluate numerically. To a large extent, this is due to the partial-wave expansion that inevitably appears in the evaluation of the function $G^{(2+)}$. The convergence of this expansion is rather good for the ground state of high-Z ions (provided that radial integrations are carried out first), but quickly worsens when Z is decreased and(or) the principal quantum number n is increased. An approach to overcome this difficulty was suggested in Ref. [34]. It is based on the separation of the ≥ 2-potential Green function $G^{(2+)}$ into two parts,

$$\begin{aligned} G^{(2+)}(\varepsilon, \boldsymbol{x}_1, \boldsymbol{x}_2) \;=\; & G^{(2+)}_a(\varepsilon, \boldsymbol{x}_1, \boldsymbol{x}_2) \\ & + \left[G^{(2+)}(\varepsilon, \boldsymbol{x}_1, \boldsymbol{x}_2) - G^{(2+)}_a(\varepsilon, \boldsymbol{x}_1, \boldsymbol{x}_2)\right], \end{aligned} \tag{13}$$

where $G^{(2+)}_a$ yields an approximation to $G^{(2+)}$ in the region where $\boldsymbol{x}_1 \approx \boldsymbol{x}_2$ and the energy argument is far away from a pole. This separation is related to the one used in Ref. [35] for the identification of ultraviolet divergent parts of the SE operator in coordinate space. The function $G^{(2+)}_a$ is given by

$$\begin{aligned} G^{(2+)}_a(\varepsilon, \boldsymbol{x}_1, \boldsymbol{x}_2) = {} & G^{(0)}(\varepsilon + \Omega, \boldsymbol{x}_1, \boldsymbol{x}_2) - G^{(0)}(\varepsilon, \boldsymbol{x}_1, \boldsymbol{x}_2) \\ & - \Omega\, \frac{\partial}{\partial E}\, G^{(0)}(E, \boldsymbol{x}_1, \boldsymbol{x}_2)\Big|_{E=\varepsilon}\,, \end{aligned} \tag{14}$$

where $G^{(0)}$ is the free Dirac Green function and $\Omega = 2Z\alpha/(x_1 + x_2)$. The function $G^{(2+)}_a$ has two important properties: (i) it can be easily expressed both in the closed form and in the partial-wave expansion form and (ii) it depends on angular variables through $\boldsymbol{x}_{12} = \boldsymbol{x}_1 - \boldsymbol{x}_2$ only. These features ensure that the numerical evaluation of expressions with $G^{(2+)}_a$ is rather simple. The main reason to introduce the auxiliary function $G^{(2+)}_a$ is that the separation (13) improves the convergence of the partial-wave expansion. It was demonstrated in Ref. [34] that the substitution of the difference $G^{(2+)} - G^{(2+)}_a$ into (the high-energy part of) Eq. (8) improves the convergence of the partial-wave expansion drastically and allows one to obtain reasonably accurate results for the SE correction at $Z = 1$ with employing just about 30 partial waves. This approach was extensively used in the present work for the evaluation of the two-loop corrections. Its usage allowed us to obtain accurate numerical results for the whole region of the nuclear charge numbers $Z = 1 - 100$ in calculations of the diagrams in Fig. 1(d)-(f) and (k).

B. Vacuum-polarization

The one-loop vacuum-polarization (VP) potential consists of two parts, which are commonly referred to as the

Uehling and the Wichmann-Kroll ones, see the review [36] for details,

$$U_{\rm VP}(r) = U_{\rm Ueh}(r) + U_{\rm WK}(r)\,. \tag{15}$$

The expression for the Uehling potential is given by

$$U_{\rm Ueh}(r) \;= -\frac{2\alpha^2 Z}{3mr}\int_0^\infty dr' r' \rho(r') \times \left[K_0(2m|r-r'|) - K_0(2m|r+r'|)\right]\,, \tag{16}$$

where

$$K_0(x) = \int_1^\infty dt\, e^{-xt}\left(\frac{1}{t^3}+\frac{1}{2t^5}\right)\sqrt{t^2-1}\,, \tag{17}$$

and the nuclear-charge density $\rho(\boldsymbol{r})$ is spherically symmetric and normalized by the condition $\int d\boldsymbol{r}\,\rho(\boldsymbol{r}) = 1$. The Wichmann-Kroll potential is conveniently expressed in terms of the VP charge density $\rho_{\rm VP}^{(3+)}(r)$,

$$U_{\rm WK}(r) = \int_0^\infty dr'\, r'^2\,\frac{1}{r_>}\,\rho_{\rm VP}^{(3+)}(r')\,, \tag{18}$$

where $r_> = \max(r,r')$. The VP charge density can be written as

$$\rho_{\rm VP}^{(3+)}(r) = \frac{2\alpha}{\pi}\,{\rm Re}\,\sum_\kappa |\kappa| \int_0^\infty d\omega\,{\rm Tr}\,G_\kappa^{(3+)}(i\omega,r,r)\,, \tag{19}$$

where $G_\kappa^{(3+)}$ denotes the radial part of the electron propagator that contains three and more interactions with the binding Coulomb field and κ is the relativistic angular quantum number. It was shown [37, 38] that no spurious terms arise in a numerical evaluation of Eq. (19) if the expansion over κ is terminated by a finite cutoff parameter.

According to the Furry theorem, all parts of the electron propagator that contain an even number of interactions with the binding field yield a vanishing contribution to the VP charge density. Thus, in numerical evaluations, the function $G_\kappa^{(3+)}$ in Eq. (19) can be substituted by $G_\kappa^{(2+)}$, which is conveniently expressed as

$$G_\kappa^{(2+)}(\omega,x,y) = \int_0^\infty dz\, z^2\, G_\kappa^{(0)}(\omega,x,z)\,V(z) \times \left[G_\kappa(\omega,z,y) - G_\kappa^{(0)}(\omega,z,y)\right]\,, \tag{20}$$

where G_κ is the radial part of the bound-electron propagator, $G_\kappa^{(0)}$ is the radial part of the free electron propagator, and $V(z)$ is the binding potential.

Formulas (16)-(20) were employed for the numerical evaluation of the one-loop VP potential in this work, using the numerical procedure developed in Refs. [38, 39]. The Uehling potential was calculated with the Fermi model of the nuclear-charge distribution, whereas for the Wichmann-Kroll potential, the spherical shell model [$\rho(r) \propto \delta(r-R)$] was employed. The summation over κ in Eq. (19) was extended up to $|\kappa_{\rm max}| = 10$.

We mention that in the case when high numerical accuracy is not needed and the finite nuclear size correction may be disregarded, the Wichmann-Kroll potential can be conveniently evaluated by employing analytical approximation formulas reported in Ref. [40].

II. TWO-LOOP QED CORRECTIONS

The two-loop contributions to the energy shift are conveniently represented in terms of the dimensionless function $F(Z\alpha)$ defined by

$$\Delta E = m\left(\frac{\alpha}{\pi}\right)^2\frac{(Z\,\alpha)^4}{n^3}\,F(Z\,\alpha)\,, \tag{21}$$

where n is the principal quantum number.

A. Self-energy in the Coulomb potential modified by the vacuum polarization

We start our consideration of the two-loop corrections with the set of the three diagrams in Fig. 1(d)-(f). This set is gauge invariant and can be regarded as the one-loop SE correction in the combined field of the nuclear Coulomb and the VP potential. The corresponding energy shift will be referred to as the SEVP correction in the following.

Formal expressions for the SEVP correction can be obtained by considering the first-order perturbation of the one-loop SE correction by the VP potential (15). Perturbations of the reference-state wave function, the binding energy, and the electron propagator give rise to the irreducible, the reducible, and the vertex contributions, respectively. The irreducible part is

$$\Delta E_{\rm SEVP}^{\rm ir} = \langle a|\gamma^0\Sigma_R(\varepsilon_a)|\delta a\rangle + \langle \delta a|\gamma^0\Sigma_R(\varepsilon_a)|a\rangle\,, \tag{22}$$

where Σ_R is the renormalized SE operator, and $|\delta a\rangle$ is the first-order perturbation of the reference-state wave function $|a\rangle$ by $U_{\rm VP}$. The reducible part is given by

$$\Delta E_{\rm SEVP}^{\rm red} = \langle a|U_{\rm VP}|a\rangle\;\langle a|\gamma_0\,\frac{\partial}{\partial\varepsilon}\Sigma_R(\varepsilon)|a\rangle\Big|_{\varepsilon=\varepsilon_a}\,, \tag{23}$$

and the vertex part is

$$\Delta E_{\rm SEVP}^{\rm ver} \;= 2i\alpha\int_{-\infty}^{\infty}d\omega\sum_{n_1 n_2} \times \frac{\langle n_1|U_{\rm VP}|n_2\rangle\,\langle an_2|\alpha_\mu\alpha_\nu D^{\mu\nu}(\omega)|n_1 a\rangle}{(\varepsilon_a-\omega-\varepsilon_{n_1})(\varepsilon_a-\omega-\varepsilon_{n_2})}\,, \tag{24}$$

where the summation over $n_{1,2}$ goes over the Dirac spectrum, and the virtual-state energies are assumed to have a small imaginary addition, $\varepsilon_n \to \varepsilon_n(1-i0)$.

The problem of calculating the SE correction in the presence of the perturbing potential has been extensively studied in the literature, see, e.g., Ref. [41, 42, 43, 44]. In this work, we employ the general scheme developed in our previous study [45] for the case of the SE correction to the hyperfine splitting. Several modifications were introduced into the scheme, among them the inclusion of the finite nuclear size effect. This modification was essential, firstly, because the effect is significantly enhanced by the singular behavior of the VP potential and, secondly, because the extended nuclear charge distribution removes the logarithmic singularity of the point-nucleus Uehling potential, which simplifies numerical integrations considerably. Even with the extended nuclear size, the usage of extremely fine grids was required in the nuclear region, in order to achieve a high controllable accuracy in radial integrations.

In actual calculations, the Fermi model of the nuclear-charge distribution was employed for the evaluation of the reference-state wave function and the Uehling potential, whereas the electron propagator(s) inside the SE loop and the Wichmann-Kroll potential were calculated with the spherical shell model [$\rho(r) \propto \delta(r-R)$]. For systems with $Z < 10$, we neglected the nuclear-size dependence in the electron propagators. The values of the root-mean-square (rms) radii of the nuclear-charge distribution were taken from Ref. [46] in most cases. For uranium, we used the value $\langle r^2 \rangle^{1/2} = 5.8569\,(33)$ fm obtained in the recent re-evaluation of experimental data [47]. In the case of fermium ($Z = 100$), there is no experimental results available, so we used the interpolation formula from Ref. [48] and assigned a (conventional) uncertainty of 1% to the resulting value. The rms radii used in the present investigation are listed in second column of Table I.

The calculational results for the SEVP correction for the $1s$, $2s$, $2p_{1/2}$, and $2p_{3/2}$ states of H-like ions are presented in Table I, expressed in terms of the function $F(Z\alpha)$ defined by Eq. (21). Our results are in good agreement with the values reported previously for uranium, lead, and ytterbium in Ref. [20]. The uncertainty specified in the table includes the numerical error and the estimated errors due to the models of the nuclear charge distribution and due to uncertainties of the rms radii. The model dependence of the results was estimated by switching between the Fermi, the uniform, and the spherical-shell models in evaluations of the Uehling potential and the wave functions; the largest deviation was taken as the error due to the nuclear model. The error due to the uncertainty of the nuclear radius was obtained by repeating the calculations with the rms radii varied within the error bars specified in the table. All three errors were added quadratically. In Table I and in the tables that follow, the omitted uncertainty means that the expected error is smaller than the last significant digit specified.

It is instructive to compare our nonpertubative results with the ones obtained within the $Z\alpha$-expansion approach. The $Z\alpha$ expansion of the SEVP correction reads

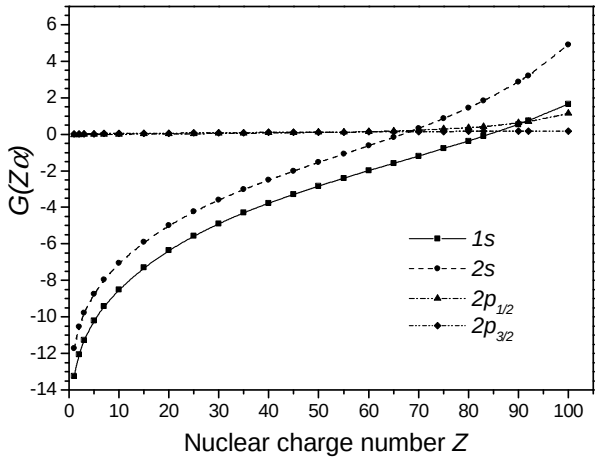

FIG. 2: Higher-order remainder $G(Z\alpha)$ for the SEVP correction. Errors due to the model of the nuclear-charge distribution and the rms radii are not shown.

$$\Delta E_{\rm SEVP} = m\left(\frac{\alpha}{\pi}\right)^2 \frac{(Z\alpha)^5}{n^3}\Big\{a_{50} + (Z\alpha)\,\ln^2\left[(Z\alpha)^{-2}\right]\,a_{62} + (Z\alpha)\,\ln\left[(Z\alpha)^{-2}\right]\,a_{61} + (Z\alpha)\,G(Z\alpha)\Big\}, \tag{25}$$

where the function $G(Z\alpha)$ is the higher-order remainder, $G(0\alpha) = a_{60}$. The results known for the coefficients of this expansion are: [14, 49, 50, 51, 52]:

$$a_{50} = 1.920576\,\delta_{l,0}\,, \tag{26}$$

$$a_{62} = \frac{4}{45}\,\delta_{l,0}\,, \tag{27}$$

$$a_{61} = \frac{16}{15}\left(\frac{2}{9} + \ln 2\right)\delta_{l,0} - \frac{32}{45}\left(\frac{3}{4} + \frac{1}{4n^2} - \frac{1}{n} + \gamma + \Psi(n) - \ln n\right)\delta_{l,0} - \frac{8}{135}\,\frac{n^2-1}{n^2}\,\delta_{l,1}\,. \tag{28}$$

The higher-order remainder $G(Z\alpha)$ was inferred from our numerical results for the SEVP correction and plotted on Fig. 2. For hydrogen, the results of our direct numerical evaluation are: $G_{1s}(\alpha) = -13.2\,(4)$, $G_{2s}(\alpha) = -11.7\,(4)$, $G_{2p_{1/2}}(\alpha) = -0.034$, and $G_{2p_{3/2}}(\alpha) = 0.015$. For the normalized difference of the $2s$ and $1s$ states and for the fine-structure difference, these values are consistent with the analytical results $a_{60}(2s) - a_{60}(1s) = 1.491199$ and $a_{60}(2p_{3/2}) - a_{60}(2p_{1/2}) = 1/20$ [52].

TABLE I: Energy shifts due the SEVP correction, in units of $F(Z\alpha)$. Uncertainties specified include the estimated errors due to the nuclear charge distribution models and the values of the rms radius.

Z	$\langle r^2\rangle^{1/2}$[fm]	$1s$	$2s$	$2p_{1/2}$	$2p_{3/2}$
1	0.879 (9)	0.01474 (2)	0.01459 (2)	−0.000025	−0.000022
2	1.676 (3)	0.02993 (2)	0.02945 (4)	−0.000086	−0.000076
3	2.43 (3)	0.04519 (3)	0.04430 (5)	−0.000175	−0.000152
5	2.41 (3)	0.07546 (4)	0.07355 (6)	−0.000414	−0.000352
7	2.558 (7)	0.10508 (3)	0.10208 (7)	−0.000715	−0.000597
10	3.005 (2)	0.14804 (3)	0.14351 (5)	−0.001242	−0.001008
15	3.189 (2)	0.21618 (3)	0.20961 (4)	−0.002206	−0.001700
20	3.476 (1)	0.28099 (5)	0.27394 (5)	−0.003130	−0.002265
25	3.706 (2)	0.34394 (4)	0.33841 (6)	−0.003868	−0.002577
30	3.929 (1)	0.40649 (5)	0.40497 (6)	−0.004269 (1)	−0.002529 (1)
35	4.163 (2)	0.47012 (3)	0.47570 (6)	−0.004161 (1)	−0.002025 (1)
40	4.270 (1)	0.53642 (4)	0.55290 (5)	−0.003332 (1)	−0.000974 (4)
45	4.494 (2)	0.60687 (3)	0.63898 (5)	−0.001500 (1)	0.000711 (2)
50	4.654 (1)	0.68338 (3)	0.73709 (5)	0.001724 (2)	0.003116 (6)
55	4.804 (5)	0.76802 (3)	0.85095 (4)	0.006884 (2)	0.00634 (1)
60	4.912 (2)	0.86337 (4)	0.98540 (4)	0.014770 (3)	0.010449 (6)
65	5.1 (2)	0.9723 (7)	1.1463 (8)	0.02653 (2)	0.015548 (8)
70	5.311 (6)	1.09812 (5)	1.34094 (6)	0.043840 (4)	0.02171 (1)
75	5.34 (1)	1.2478 (2)	1.5827 (2)	0.069408 (9)	0.029019 (10)
80	5.463 (2)	1.42573 (5)	1.8834 (2)	0.107174 (8)	0.037514 (4)
83	5.521 (3)	1.55007 (6)	2.1010 (2)	0.138236 (10)	0.043186 (7)
90	5.71 (5)	1.905 (2)	2.751 (3)	0.2488 (2)	0.05798 (3)
92	5.857 (3)	2.0238 (4)	2.9786 (8)	0.29400 (2)	0.06251 (1)
100	5.86 (6)	2.650 (4)	4.224 (8)	0.5871 (8)	0.08183 (6)

B. Two-loop vacuum polarization

The two-loop VP correction is represented by the diagrams in Fig. 1(g)-(i). (The term the "two-loop VP" will be abbreviated as "VPVP" in the following.) It will be convenient to split our evaluation of the VPVP correction into two parts, considering separately the diagram (g) and the remaining two diagrams (h) and (i).

1. Diagram (g)

The correction induced by the diagram in Fig. 1(g) can be regarded as the second-order perturbation contribution induced by the one-loop VP potential $U_{\rm VP}$,

$$\Delta E_{{\rm VPVP},\,g} = \sum_{n\neq a} \frac{\langle a|U_{\rm VP}|n\rangle\,\langle n|U_{\rm VP}|a\rangle}{\varepsilon_n - \varepsilon_a}\,. \qquad (29)$$

The numerical evaluation of this correction is relatively simple. It was carried out by employing the general scheme developed for the VP potential and described in Sec. I B. The summation over the Dirac spectrum was performed by the dual-kinetic-balance basis set method [53].

The numerical values of the energy shifts induced by the diagram in Fig. 1(g) are presented in Table II for the $n = 1$ and $n = 2$ states of H-like ions. The results are expressed in terms of the function $F(Z\alpha)$ defined by Eq. (21). Good agreement is found with the previous evaluations of this corrections [20, 22]. Our calculation accounts for the extended nuclear charge distribution (with the Fermi model employed for the Uehling potential and the wave functions and the spherical shell model, for the Wichmann-Kroll potential). The uncertainties listed in the table include the numerical error as well as the estimated errors due to the models of the nuclear charge distribution and due to the uncertainties of the values of the rms radii. The estimation of errors was done similarly to that for the SEVP correction.

The higher-order part of the correction can be identified by taking into account its $Z\alpha$ expansion of the form

$$\Delta E_{{\rm VPVP},\,g} = m\left(\frac{\alpha}{\pi}\right)^2 \frac{(Z\alpha)^5}{n^3}\Big\{a_{50} + (Z\alpha)\,\ln\left[(Z\alpha)^{-2}\right]\,a_{61} + (Z\alpha)\,G(Z\alpha)\Big\}, \qquad (30)$$

where [14, 49, 54]

$$a_{50} = -\frac{23\pi}{1134}\,\delta_{l,0}\,, \qquad (31)$$

$$a_{61} = -\frac{8}{225}\,\delta_{l,0}\,, \qquad (32)$$

and $G(Z\alpha)$ is the higher-order remainder, $G(0\alpha) = a_{60}$. The remainder $G(Z\alpha)$ inferred from our numerical results is plotted on Fig. 3. The results for hydrogen are: $G_{1s}(\alpha) = -0.115$, $G_{2s}(\alpha) = -0.059$, $|G_{2p_{1/2}}(\alpha)| < 10^{-4}$, and $|G_{2p_{3/2}}(\alpha)| < 10^{-4}$.

TABLE II: Energy shifts induced by the VPVP diagram in Fig. 1(g), in units of $F(Z\alpha)$. The uncertainties specified include the estimated errors due to the nuclear charge distribution models and due to the rms radii.

Z	$1s$	$2s$	$2p_{1/2}$	$2p_{3/2}$
1	−0.000490	−0.000487		
2	−0.001018	−0.001006		
3	−0.001578	−0.001552		
5	−0.002784	−0.002716		
7	−0.004092	−0.003967	−0.000001	
10	−0.006231	−0.005995	−0.000002	
15	−0.010260 (1)	−0.009803 (1)	−0.000009	
20	−0.014896 (1)	−0.014216 (1)	−0.000026	−0.000001
25	−0.020225 (2)	−0.019375 (2)	−0.000060	−0.000002
30	−0.026376 (3)	−0.025480 (3)	−0.000124	−0.000003
35	−0.033524 (5)	−0.032796 (5)	−0.000235	−0.000005
40	−0.041928 (8)	−0.041708 (8)	−0.000421	−0.000007
45	−0.05185 (1)	−0.05265 (1)	−0.000727	−0.000010
50	−0.06374 (2)	−0.06631 (2)	−0.001218 (1)	−0.000015
55	−0.07810 (3)	−0.08356 (3)	−0.001998 (1)	−0.000021
60	−0.09568 (5)	−0.10566 (6)	−0.003233 (2)	−0.000029
65	−0.1173 (2)	−0.1342 (3)	−0.00518 (1)	−0.000039
70	−0.1441 (1)	−0.1713 (1)	−0.008238 (7)	−0.000051
75	−0.1785 (2)	−0.2212 (2)	−0.01313 (1)	−0.000067
80	−0.2221 (3)	−0.2880 (4)	−0.02094 (3)	−0.000085
83	−0.2542 (4)	−0.3393 (5)	−0.02778 (4)	−0.000099
90	−0.3522 (9)	−0.505 (1)	−0.0543 (1)	−0.000136
92	−0.3865 (9)	−0.566 (1)	−0.0658 (1)	−0.000149
100	−0.583 (3)	−0.935 (4)	−0.1482 (6)	−0.000209

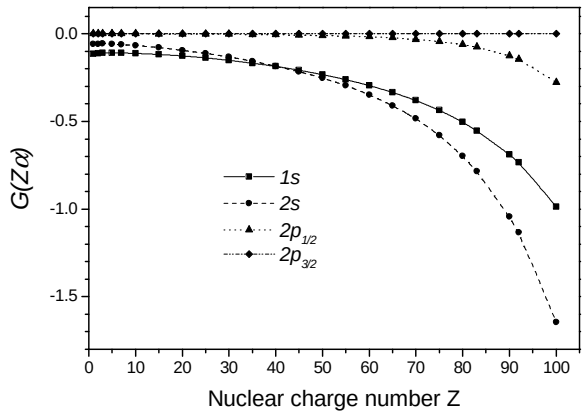

FIG. 3: Higher-order remainder $G(Z\alpha)$ induced by the diagram in Fig. 1(g).

2. Diagrams (h) and (i)

We now consider the energy shift induced by the diagrams in Fig. 1(h) and (i). Its leading (in $Z\alpha$) part can be obtained within the *free-loop* approximation, i.e., keeping the first nonvanishing term in the expansion of the fermion loop in terms of the binding potential. The corresponding expression was derived long ago in the classical paper by Källén and Sabry [55]. Later, it was re-derived by a number of other techniques [56, 57, 58]. According to the Furry theorem, corrections to the Källén-Sabry potential are suppressed by a factor of $(Z\alpha)^2$, so that this potential is supposed to yield a dominant contribution even in the medium-Z region. In the present investigation, diagrams (h) and (i) will be approached within the free-loop approximation only. In order to stress this fact, we will use the superscript "KS" in the formulas below.

In the free-loop approximation, the correction induced by the diagrams in Fig. 1(h) and (i) is given by the expectation value of the Källén-Sabry potential,

$$\Delta E^{KS}_{\mathrm{VPVP},\,hi} = \langle a|V_{KS}|a\rangle\,. \tag{33}$$

For a spherically symmetric nuclear charge distribution, the Källén-Sabry potential can be conveniently written in the form [59]

$$V_{KS}(r) = -\frac{\alpha^3 Z}{m\pi r}\int_0^\infty dr'\,r'\rho(r')\,\left[L_0(2m|r-r'|) - L_0(2m|r+r'|)\right]\,, \tag{34}$$

where

$$L_0(x) = \int_1^\infty dt\,\frac{e^{-xt}}{t}\left\{\left(-\frac{13}{54t^2}-\frac{7}{108t^4}-\frac{2}{9t^6}\right)\sqrt{t^2-1}+\left(\frac{44}{9t}-\frac{2}{3t^3}-\frac{5}{4t^5}-\frac{2}{9t^7}\right)\ln[t+\sqrt{t^2-1}]\right.$$
$$+\left(-\frac{4}{3t^2}-\frac{2}{3t^4}\right)\sqrt{t^2-1}\,\ln[8t(t^2-1)]$$
$$\left.+\left(\frac{8}{3t}-\frac{2}{3t^5}\right)\int_t^\infty dy\left(\frac{3y^2-1}{y(y^2-1)}\,\ln[y+\sqrt{y^2-1}]-\frac{1}{\sqrt{y^2-1}}\ln[8y(y^2-1)]\right)\right\}, \quad (35)$$

and the nuclear charge density is normalized by $\int d\boldsymbol{r}\,\rho(\boldsymbol{r}) = 1$.

The results of our numerical evaluation of the energy shift due to the Källén-Sabry potential are listed in Table III. The numerical values presented agree well with the results of the previous studies [18, 19]. Our calculation was carried out with employing the Fermi model for the nuclear charge distribution. The values for the rms radii and their uncertainties are listed in Table I. The uncertainties specified in Table III for our numerical results include the numerical error as well as the errors due to the nuclear-charge distribution model and due to uncertainties of the rms radii. The error due to the nuclear model was estimated by taking the difference of the results obtained with the Fermi and the uniform model.

The $Z\alpha$ expansion of the Källén-Sabry contribution reads

$$\Delta E^{KS}_{\mathrm{VPVP},\,hi} = m\left(\frac{\alpha}{\pi}\right)^2\frac{(Z\alpha)^4}{n^3}\Big\{a_{40}+(Z\alpha)\,a_{50}$$
$$+(Z\alpha)^2\,\ln\left[(Z\alpha)^{-2}\right]\,a_{61}+(Z\alpha)^2\,G(Z\alpha)\Big\}, \quad (36)$$

where the function $G(Z\alpha)$ is the higher-order remainder. The results for the first terms of the $Z\alpha$ expansion are [14, 49, 54, 60, 63]:

$$a_{40} = -\frac{82}{81}\,\delta_{l0}\,, \quad (37)$$
$$a_{50} = \left(\frac{45331}{39690}-\frac{25}{63}\pi+\frac{52}{63}\ln 2\right)\pi\,\delta_{l0}\,, \quad (38)$$
$$a_{61} = \frac{a_{40}}{2}\,. \quad (39)$$

The higher-order remainder $G(Z\alpha)$ inferred from the Källén-Sabry contribution is plotted as a function of the nuclear charge number Z on Fig. 4. For hydrogen, the results for the Källén-Sabry remainder term are: $G_{1s}(\alpha) = -2.642$, $G_{2s}(\alpha) = -3.303$, $G_{2p_{1/2}}(\alpha) = -0.263$, and $G_{2p_{3/2}}(\alpha) = -0.073$.

Our numerical results for the higher-order remainder for the *total* VPVP correction exhibit good agreement with the analytical values obtained in Ref. [52] for the normalized difference of the $2s$ and $1s$ states and for the fine-structure difference. Indeed, for the VPVP remainder, our calculation yields: $G_{2s}(\alpha) - G_{1s}(\alpha) = -0.605$ and $G_{2p_{3/2}}(\alpha) - G_{2p_{1/2}}(\alpha) = 0.190$, to be compared with the analytical results of $a_{60}(2s) - a_{60}(1s) = -0.611365$ and $a_{60}(2p_{3/2}) - a_{60}(2p_{1/2}) = 0.189815$, correspondingly.

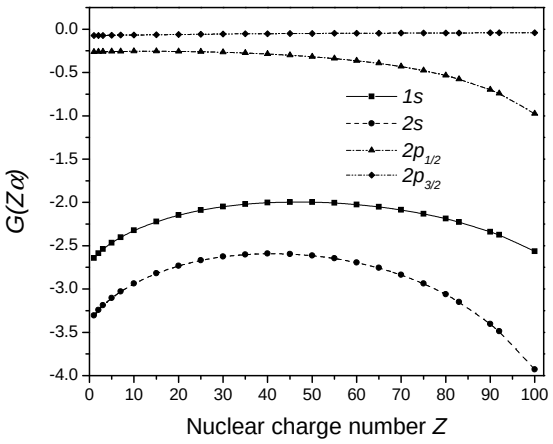

FIG. 4: Higher-order remainder $G(Z\alpha)$ induced by the Källén-Sabry contribution.

A complete evaluation of the VPVP correction beyond the free-loop approximation is a difficult problem [especially, for diagram (i)] and has not been carried out up to now. For diagram (h), the calculation is easier and can be performed by a generalization of methods developed for the one-loop VP correction. For uranium and lead, such a calculation was reported in Ref. [23]. The numerical values obtained for this diagram for the contribution beyond the free-loop approximation turned out to be rather small; it is expected that the corresponding contribution from diagram (i) is much larger. In the absence of a direct calculation, we estimate the theoretical uncertainty of the VPVP correction due to the omitted part beyond the free-loop approximation by multiplying the absolute value of the Källén-Sabry contribution by a factor of $(Z\alpha)^2$.

C. Vacuum-polarization insertion into the self-energy photon line

In this section, we address the correction induced by the SE diagram with the VP insertion into the photon

TABLE III: Energy shifts due to the Källén-Sabry potential, in units of $F(Z\alpha)$. The uncertainties specified include the estimated errors due to the nuclear charge distribution models and due to the rms radii.

Z	$1s$	$2s$	$2p_{1/2}$	$2p_{3/2}$
1	−1.002032	−1.002067	−0.000014	−0.000004
2	−0.992369	−0.992509	−0.000056	−0.000015
3	−0.983258	−0.983568	−0.000125	−0.000034
5	−0.966493	−0.967341	−0.000344	−0.000093
7	−0.951435	−0.953071	−0.000670	−0.000179
10	−0.931629	−0.934898	−0.001360	−0.000354
15	−0.904993 (1)	−0.912148	−0.003055	−0.000757
20	−0.885141 (1)	−0.897624 (1)	−0.005471	−0.001287
25	−0.871198 (1)	−0.890494 (1)	−0.008683	−0.001927
30	−0.862607 (2)	−0.890315 (2)	−0.012801	−0.002669
35	−0.859040 (3)	−0.896935 (3)	−0.017978	−0.003504
40	−0.860403 (4)	−0.910519 (5)	−0.024416	−0.004426
45	−0.866633 (6)	−0.931345 (7)	−0.032384	−0.005431
50	−0.877972 (8)	−0.960119 (9)	−0.042236	−0.006517
55	−0.89473 (1)	−0.99776 (1)	−0.054441	−0.007684
60	−0.91747 (2)	−1.04561 (2)	−0.069624 (1)	−0.008931
65	−0.9468 (3)	−1.1053 (4)	−0.08862 (1)	−0.010259
70	−0.98346 (4)	−1.17895 (4)	−0.112569 (2)	−0.011673
75	−1.02957 (7)	−1.27069 (9)	−0.143102 (5)	−0.013175
80	−1.08601 (7)	−1.38369 (9)	−0.182409 (7)	−0.014770
83	−1.12595 (8)	−1.4642 (1)	−0.21150 (1)	−0.015775
90	−1.2402 (5)	−1.6988 (8)	−0.30171 (8)	−0.018267
92	−1.2784 (2)	−1.7791 (2)	−0.33488 (3)	−0.019020
100	−1.476 (1)	−2.201 (2)	−0.5202 (3)	−0.022227

line, depicted by Fig. 1(k). The corresponding shift of the energy will be referred to as the S(VP)E correction. The leading (in $Z\alpha$) part of this correction can be again obtained within the free-loop approximation. Unlike the VPVP contribution, however, corrections to the free-loop approximation in this case are suppressed only by the first power of $Z\alpha$. The leading term beyond this approximation is known from perturbative calculations [49, 64]. An all-order calculation of the S(VP)E correction beyond the free-loop approximation is a difficult problem and has not been performed so far. In the present investigation, we will approach the S(VP)E correction within the free-loop approximation only.

The evaluation of the S(VP)E correction within the free-loop approximation can be performed by a generalization of the method for the one-loop SE correction described in Section I A. The S(VP)E correction is represented by a sum of the zero-, one-, and many-potential terms:

$$\Delta E_{\rm SVPE,a} = \Delta E^{(0)}_{\rm SVPE,a} + \Delta E^{(1)}_{\rm SVPE,a} + \Delta E^{(2+)}_{\rm SVPE,a}\,, \quad (40)$$

where the subscript "a" indicates the free-loop approximation. Formulas for the three terms above can be obtained from the corresponding expressions in Section I A by replacing the standard photon propagator by the "dressed" one, obtained by inserting the renormalized one-loop VP tensor into the photon line. In $D = 4 - 2\epsilon$ dimensions, the replacement is given by [21, 65]

$$\frac{1}{k^2 + i0} \to -\frac{\alpha C_\epsilon}{4\pi}\, m^{2\epsilon} \int_0^1 dz\, \frac{z^2(1 - z^2/3)}{[m^2 - k^2(1 - z^2)/4 - i0]^{1+\epsilon}}\,, \quad (41)$$

where $C_\epsilon = (4\pi)^\epsilon\, \Gamma(1 + \epsilon)\, \mu^{2\epsilon}/m^{2\epsilon}$.

The zero-potential term is represented by

$$\Delta E^{(0)}_{\rm SVPE,a} = \int \frac{d\boldsymbol{p}}{(2\pi)^3}\, \overline{\psi}_a(\boldsymbol{p})\, \Sigma^{(0)}_{\rm VP,R}(\varepsilon_a, \boldsymbol{p})\, \psi_a(\boldsymbol{p})\,, \quad (42)$$

where the free dressed SE operator $\Sigma^{(0)}_{\rm VP}$ is obtained from Eq. (9) by the substitution (41), and its renormalized part $\Sigma^{(0)}_{\rm VP,R}$ is the finite part of the difference $\Sigma^{(0)}_{\rm VP} - \delta m$ when ϵ approaches zero. Applying the standard technique for the evaluation of momentum integrals (see, e.g., Appendices of Ref. [28]), the difference $\Sigma^{(0)}_{\rm VP} - \delta m$ is conveniently represented as

$$\Sigma^{(0)}_{\rm VP}(p) - \delta m \;=\; \left(\frac{\alpha C_\epsilon}{4\pi}\right)^2 \left[-\frac{2}{3\epsilon^2} + \frac{13}{9\epsilon} - \frac{599}{54} + \frac{8\pi^2}{9}\right](\not{p} - m)$$
$$+ \left(\frac{\alpha}{4\pi}\right)^2 8 \int_0^1 dx\, dz\, \frac{z^2(1-z^2/3)}{1-z^2}\big[(1-x)\not{p} - 2m\big]\, \ln\frac{x(1-z^2)Y + 4(1-x)}{x^2(1-z^2)+4(1-x)}\,, \qquad (43)$$

where $Y = x(1-\rho)+\rho$ and $\rho = (m^2-p^2)/m^2$.

The one-potential term is given by

$$\Delta E^{(1)}_{\rm SVPE,a} \;=\; \int \frac{d\boldsymbol{p}_1}{(2\pi)^3}\,\frac{d\boldsymbol{p}_2}{(2\pi)^3}\,\overline{\psi}_a(\boldsymbol{p}_1)$$
$$\times \Gamma^0_{\rm VP,R}(\varepsilon_a,\boldsymbol{p}_1;\varepsilon_a,\boldsymbol{p}_2)\, V_C(\boldsymbol{q})\, \psi_a(\boldsymbol{p}_2)\,, \qquad (44)$$

where $\Gamma^0_{\rm VP,R}$ is the finite (when $\epsilon \to 0$) part of the time component of the dressed vertex operator $\Gamma^\alpha_{\rm VP}$, which is obtained from the one-loop vertex operator Γ^α, Eq. (11), by the substitution (41). Evaluating the momentum integrations, we obtain the following representation for the operator $\Gamma^\alpha_{\rm VP}$,

$$\Gamma^\alpha_{\rm VP}(p_1,p_2) = \left(\frac{\alpha C_\epsilon}{4\pi}\right)^2 \gamma^\alpha \left(\frac{2}{3\epsilon^2} - \frac{13}{9\epsilon} - \frac{877}{54} + \frac{16\pi^2}{9}\right)$$
$$- \left(\frac{\alpha}{4\pi}\right)^2 \int_0^1 dx\, dy\, dz\, xz^2 \left(1 - \frac{z^2}{3}\right)\left\{\frac{4\,N^\alpha(xb)}{x(1-z^2)D + 4m^2(1-x)} + \frac{8\,\gamma^\alpha}{1-z^2}\,\ln\frac{x(1-z^2)D/m^2 + 4(1-x)}{x^2(1-z^2)+4(1-x)}\right\}, \qquad (45)$$

where $D = xb^2 + m^2 - yp_1^2 - (1-y)p_2^2$, $b = yp_1 + (1-y)p_2$, and $N^\alpha(k) = \gamma_\sigma(\not{p}_1 - \not{k} + m)\gamma^\alpha(\not{p}_2 - \not{k} + m)\gamma^\sigma$. Using the Ward identity, it is easy to check that the divergent parts of Eqs. (45) and (43) (i.e., terms $\sim \epsilon^{-1}$ and ϵ^{-2}) cancel each other in the total expression for the energy shift. This is the justification of our definition of the renormalized parts of the operators $\Sigma^{(0)}_{\rm VP}$ and $\Gamma^\alpha_{\rm VP}$, which consists just in dropping out the divergent part of Eqs. (43) and (45).

The numerical evaluation of the zero- and one-potential terms is similar to that for the one-loop SE correction but is more time consuming, due to the presence of additional integrations over Feynman parameters. In order to achieve high numerical accuracy for the one-potential term in the low-Z region, we had to identify the contribution of Eq. (45) at $p_1 = p_2$ and evaluate it separately. The subtraction of this contribution in Eq. (44) makes the integrand to be a smooth function at $q = 0$, which simplifies numerical integrations considerably.

The many-potential term is given by

$$\Delta E^{(2+)}_{\rm SVPE,a} = 2i\alpha \int_{-\infty}^{\infty} d\omega \int d\boldsymbol{x}_1\, d\boldsymbol{x}_2\, D^{\mu\nu}_{VP}(\omega,\boldsymbol{x}_{12})$$
$$\times\, \psi^\dagger_a(\boldsymbol{x}_1)\,\alpha_\mu\, G^{(2+)}(\varepsilon_a - \omega, \boldsymbol{x}_1, \boldsymbol{x}_2)\,\alpha_\nu\,\psi_a(\boldsymbol{x}_2)\,. \qquad (46)$$

This formula differs from the expression for the many-potential part of the one-loop SE correction only by the dressed photon propagator $D^{\mu\nu}_{VP}$, which reads

$$D^{\mu\nu}_{VP}(\omega,\boldsymbol{x}_{12}) = \frac{\alpha}{\pi}\int_1^\infty dt\;\sqrt{t^2-1}\;\frac{2t^2+1}{3t^4}$$
$$\times\, D^{\mu\nu}(\omega,\boldsymbol{x}_{12};2mt)\,. \qquad (47)$$

$D^{\mu\nu}(\omega,\boldsymbol{x};\lambda)$ is the propagator of the photon with a mass λ, whose expression in the Feynman gauge is

$$D^{\mu\nu}(\omega,\boldsymbol{x}_{12};\lambda) = g^{\mu\nu}\,\frac{\exp[i\sqrt{\omega^2-\lambda^2+i0}\,x_{12}]}{4\pi\,x_{12}}\,. \qquad (48)$$

It is easy to see that the numerical calculation of the many-potential term falls naturally into two steps: (i) the evaluation of the many-potential part of the one-loop SE correction with an effective photon mass $\lambda = 2mt$ and (ii) the numerical integration over t as given by Eq. (47). There is even a certain simplification as compared to the one-loop case. It is a common approach to deform the contour of the ω integration in Eq. (46), separating it into the low-energy and the high-energy part (see, e.g., Ref. [33] for details). In the case of the S(VP)E correction, the contribution induced by the low-energy part of the contour vanishes identically, which is due to the condition on the effective photon mass $\lambda \geq 2m$.

The results of our numerical evaluation of the S(VP)E correction for the $n = 1$ and $n = 2$ states of H-like ions are presented in Table IV. Our numerical results are in good agreement with the data obtained previously for the $1s$ state [20, 21] and with the $2s$ and $2p_{1/2}$ values for $Z = 92$ from Ref. [20]. Our calculation was performed within the

free-loop approximation and for the point nuclear model. The uncertainty specified in the table is the numerical error only. We estimate the theoretical uncertainty due to uncalculated terms beyond the free-loop approximation by multiplying the absolute value of the correction by a factor of $3\,(Z\alpha)$. This factor arises as a ratio of the leading-order contribution beyond the free-loop approximation for the $1s$ state, $-0.386\,m(\alpha/\pi)^2(Z\alpha)^5$ [49], and the leading-order contribution within this approximation, $0.142\,m(\alpha/\pi)^2(Z\alpha)^4$ [60].

The inclusion of the finite nuclear size (FNS) effect is not necessary at present for the S(VP)E correction, since it is expected to yield a much smaller contribution than the error due to the free-loop approximation. The relative contribution of the FNS effect on the S(VP)E correction can be estimated by taking the relative values of this effect for the one-loop SE correction. To the leading orders in $Z\alpha$ and $\ln R$, the relative value of the FNS-SE effect for the ns states is [61, 62]

$$\delta_{FNS} = -\alpha\left[Z\alpha\left(\frac{23}{4}-4\ln 2\right) + \frac{(Z\alpha)^2}{\pi}\left(\frac{15}{4}-\frac{\pi^2}{6}\right)\ln(b/R)\right], \qquad (49)$$

where $b=\exp[1/(2\gamma)-C-5/6]$, $\gamma=\sqrt{1-(Z\alpha)^2}$, $C\approx 0.557$ is the Euler constant, and R is the nuclear radius. Analogous formulas for the $np_{1/2}$ and $np_{3/2}$ states can be found in Ref. [62]. Numerical values of δ_{FNS} are within 3% for the whole region of the nuclear charge numbers.

The $Z\alpha$ expansion of the S(VP)E correction within the free-loop approximation reads

$$\Delta E_{\rm SVPE,a} = m\left(\frac{\alpha}{\pi}\right)^2\frac{(Z\alpha)^4}{n^3}\Big\{a_{40}+(Z\alpha)\,a_{50} + (Z\alpha)^2\ln\left[(Z\alpha)^{-2}\right]a_{61}+(Z\alpha)^2\,G(Z\alpha)\Big\}, \qquad (50)$$

where the function $G(Z\alpha)$ is the higher-order remainder. The results for the first terms of the $Z\alpha$ expansion are [14, 49, 60, 63, 64]:

$$a_{40} = \left(-\frac{7}{81}+\frac{5\pi^2}{216}\right)\delta_{l0} + \left(\frac{119}{36}-\frac{\pi^2}{3}\right)\frac{j(j+1)-l(l+1)-3/4}{l(l+1)(2l+1)}(1-\delta_{l0}), \qquad (51)$$

$$a_{50} = -0.229053\,\delta_{l0}, \qquad (52)$$

$$a_{61} = \frac{a_{40}}{2}\,\delta_{l0}. \qquad (53)$$

The higher-order remainder $G(Z\alpha)$ inferred from our numerical results is plotted in Fig. 5. For hydrogen, our results are: $G_{1s}(\alpha)=0.93\,(6)$, $G_{2s}(\alpha)=1.04\,(5)$, $G_{2p_{1/2}}(\alpha)=0.02\,(4)$, and $G_{2p_{3/2}}(\alpha)=0.01\,(3)$. These values are consistent with the $Z\alpha$-expansion results for the normalized difference of the $2s$ and $1s$ states and for the fine-structure difference [52]: $a_{60}(2s)-a_{60}(1s)=0.109999$ and $a_{60}(2p_{3/2})-a_{60}(2p_{1/2})=-0.013435$.

TABLE IV: Energy shifts due the S(VP)E correction evaluated within the free-loop approximation and for the point nucleus, in units of $F(Z\alpha)$.

Z	$1s$	$2s$	$2p_{1/2}$	$2p_{3/2}$
1	0.140459 (4)	0.140465 (3)	−0.005228 (2)	0.002615 (2)
2	0.139002 (4)	0.139026 (2)	−0.005226 (1)	0.002615 (1)
3	0.137650 (4)	0.137705 (2)	−0.005223 (1)	0.002615 (1)
5	0.135219 (4)	0.135370 (2)	−0.005212 (1)	0.002614 (1)
7	0.133099 (3)	0.133390 (4)	−0.005196 (3)	0.002612 (3)
10	0.13042 (1)	0.13100 (1)	−0.00516	0.00260
15	0.12708 (1)	0.12835 (1)	−0.00507	0.00259
20	0.12493 (1)	0.12715 (1)	−0.00492	0.00258
25	0.12381	0.12727	−0.00471	0.00255
30	0.12366	0.12866	−0.00442	0.00252
35	0.12444	0.13134	−0.00403	0.00249
40	0.12615	0.13536 (1)	−0.00350	0.00246
45	0.12882	0.14085 (1)	−0.00280	0.00242
50	0.13254	0.14801 (1)	−0.00187	0.00237
55	0.13742	0.15711 (1)	−0.00064	0.00232
60	0.14362	0.16851 (1)	0.00098	0.00226
65	0.15137	0.18271 (1)	0.00314	0.00220
70	0.16099 (1)	0.20042 (1)	0.00603	0.00213
75	0.17291 (1)	0.22260 (1)	0.00994	0.00205
80	0.18773 (1)	0.25059 (2)	0.01528	0.00197
83	0.19835 (1)	0.27097 (2)	0.01943	0.00191
90	0.22987 (2)	0.33285 (3)	0.03322	0.00177
92	0.24110 (2)	0.35535 (3)	0.03863	0.00172
100	0.30064 (3)	0.47842 (6)	0.07124 (1)	0.00152

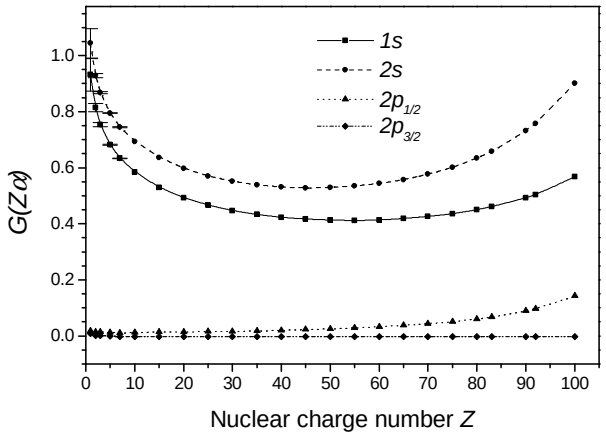

FIG. 5: Higher-order remainder $G(Z\alpha)$ for the S(VP)E correction within the free-loop approximation.

For completeness, we specify also the result for the leading term of the $Z\alpha$ expansion known for the S(VP)E correction beyond the free-loop approximation [49, 64],

$$\Delta E_{\rm SVPE,b} = m\left(\frac{\alpha}{\pi}\right)^2\frac{(Z\alpha)^5}{n^3}\left[-0.38615\,\delta_{l0}\right]. \qquad (54)$$

III. CONCLUSION

In the present investigation, we performed calculations of the part of the two-loop Lamb shift induced by the diagrams in Fig. 1(d)-(k). Numerical results were obtained for the $n = 1$ and $n = 2$ states and for the whole region of the nuclear charge numbers $Z = 1 - 100$. The diagrams (d)-(g) were calculated rigorously to all orders in $Z\alpha$, whereas for the diagrams (h)-(k), the fermion loops were approximated by their leading $Z\alpha$-expansion contribution. An estimate was given for the higher-order terms thus omitted. The finite nuclear size effect was accounted for in the evaluations of all diagrams except for the diagram (k). The latter diagram was calculated with the point nuclear model; an estimate of the finite nuclear size effect was supplied.

In the low-Z region, our numerical results were employed for the identification of the nonperturbative remainder $G(Z\alpha)$, which incorporates all orders in the $Z\alpha$-expansion starting with $\alpha^2(Z\alpha)^6$. For hydrogen, the net result for the two-loop diagrams with closed fermion loops is

$$G_{1s}(\alpha) = -15.0(4)(2.2)\,, \quad (55)$$

$$G_{2s}(\alpha) = -14.0(4)(2.2)\,, \quad (56)$$

$$G_{2p_{1/2}}(\alpha) = -0.28(4)\,, \quad (57)$$

$$G_{2p_{3/2}}(\alpha) = -0.05(3)\,, \quad (58)$$

where the first error quoted is the numerical uncertainty. The second error (if given) is due to contributions beyond the free-loop approximation. We estimate them for the ns states as 1 [in units of $G(Z\alpha)$] for the VPVP correction and as 2 for the S(VP)E diagram (which arises as a typical coefficient of 0.2 enhanced by the first power of logarithm). It is interesting to note that the dominant part of the remainder term for the ns states is due to the SEVP correction [Fig. 1(d)-(f)].

In order to get the complete results for the two-loop Lamb shift, one should combine the numerical values obtained in the present work with the contribution due to the two-loop self-energy [Fig. 1(a)-(c)]. Its all-order calculation was accomplished in our previous investigations, in Refs. [27, 28, 29, 30] for the $1s$ state and $Z \geq 10$ and in Ref. [31] for the $n = 2$ states and $Z \geq 60$. Combined together, our calculations yield results for the total two-loop QED correction, which improve the total theoretical accuracy of the $1s$ Lamb shift [27] and that of the $2p_{1/2,3/2} - 2s$ transition energy in heavy Li-like ions [31].

Still, the project of the calculation of the two-loop Lamb shift is far from being finished. There are several reasons for this. First, the results of the all-order calculation of the two-loop self-energy correction for the $1s$ state in the low-Z region [29] do not agree well with the $Z\alpha$-expansion result of Ref. [16]. Second, the calculation [31] for the $n = 2$ states was performed in the high-Z region only. Third, a part of the two-loop diagrams with closed fermion loops is presently calculated within the free-loop approximation only. Each of these points represents a difficult problem and all of them should be solved before the calculation of the Lamb shift to order α^2 is completed.

Valuable discussions with K. Pachucki and U. D. Jentschura are gratefully acknowledged. V.A.Y. acknowledges support from RFBR (grant No. 06-02-04007) and the foundation "Dynasty." Laboratoire Kastler Brossel is Unité Mixte de Recherche du CNRS n° 8552, of the Physics Department of École Normale Supérieure and Université Pierre et Marie Curie.

[1] T. Stöhlker, P. H. Mokler, K. Beckert, F. Bosch, H. Eickhoff, B. Franzke, M. Jung, T. Kandler, O. Klepper, C. Kozhuharov, R. Moshammer, F. Nolden, H. Reich, P. Rymuza, P. Spädtke, and M. Steck, Phys. Rev. Lett. **71**, 2184 (1993).

[2] T. Stöhlker, P. H. Mokler, F. Bosch, R. W. Dunford, F. Franzke, O. Klepper, C. Kozhuharov, T. Ludziejewski, F. Nolden, H. Reich, P. Rymuza, Z. Stachura, M. Steck, P. Swiat, and A. Warczak, Phys. Rev. Lett. **85**, 3109 (2000).

[3] A. Gumberidze, T. Stöhlker, D. Banaś, K. Beckert, P. Beller, H. F. Beyer, F. Bosch, S. Hagmann, C. Kozhuharov, D. Liesen, F. Nolden, X. Ma, P. H. Mokler, M. Steck, D. Sierpowski, and S. Tashenov, Phys. Rev. Lett. **94**, 223001 (2005).

[4] J. Schweppe, A. Belkacem, L. Blumenfeld, N. Claytor, B. Feinberg, H. Gould, V. E. Kostroun, L. Levy, S. Misawa, J. R. Mowat, and M. H. Prior, Phys. Rev. Lett. **66**, 1434 (1991).

[5] P. Beiersdorfer, A. L. Osterheld, J. H. Scofield, J. R. Crespo López-Urrutia, and K. Widmann, Phys. Rev. Lett. **80**, 3022 (1998).

[6] P. Bosselmann, U. Staude, D. Horn, K.-H. Schartner, F. Folkmann, A. E. Livingston, and P. H. Mokler, Phys. Rev. A **59**, 1874 (1999).

[7] C. Brandau, C. Kozhuharov, A. Müller, W. Shi, S. Schippers, T. Bartsch, S. Bohm, C. Bohme, A. Hoffknecht, H. Knopp, N. Grün, W. Scheid, T. Steih, F. Bosch, B. Franzke, P. H. Mokler, F. Nolden, M. Steck, T. Stöhlker, and Z. Stachura, Phys. Rev. Lett. **91**, 073202 (2003).

[8] P. Beiersdorfer, H. Chen, D. B. Thorn, and E. Träbert, Phys. Rev. Lett. **95**, 233003 (2005).

[9] V. A. Yerokhin, A. N. Artemyev, V. M. Shabaev, M. M. Sysak, O. M. Zherebtsov, and G. Soff, Phys. Rev. Lett. **85**, 4699 (2000).

[10] J. Sapirstein and K. T. Cheng, Phys. Rev. A **64**, 022502 (2001).

[11] M. Niering, R. Holzwarth, J. Reichert, P. Pokasov, T. Udem, M. Weitz, T. W. Hänsch, P. Lemonde, G. Santarelli, M. Abgrall, P. Laurent, C. Salomon, and A. Clairon, Phys. Rev. Lett. **84**, 5496 (2000).

[12] M. Fischer, N. Kolachevsky, M. Zimmermann, R. Holzwarth, T. Udem, T. W. Hänsch, M. Abgrall, J. Grunert, I. Maksimovic, S. Bize, H. Marion, F. P. D. Santos, P. Lemonde, G. Santarelli, P. Laurent, A. Clairon, C. Salomon, M. Haas, U. D. Jentschura, and C. H. Keitel, Phys. Rev. Lett. **92**, 230802 (2004).

[13] P. J. Mohr and B. N. Taylor, Rev. Mod. Phys. **77**, 1 (2005).

[14] K. Pachucki, Phys. Rev. A **63**, 042503 (2001).

[15] U. D. Jentschura and K. Pachucki, J. Phys. A **35**, 1927 (2002).

[16] K. Pachucki and U. D. Jentschura, Phys. Rev. Lett. **91**, 113005 (2003).

[17] A. Czarnecki, U. D. Jentschura, and K. Pachucki, Phys. Rev. Lett. **95**, 180404 (2005).

[18] T. Beier and G. Soff, Z. Phys. D **8**, 129 (1988).

[19] S. M. Schneider, W. Greiner, and G. Soff, J. Phys. B **26**, L529 (1993).

[20] H. Persson, I. Lindgren, L. N. Labzowsky, G. Plunien, T. Beier, and G. Soff, Phys. Rev. A **54**, 2805 (1996).

[21] S. Mallampalli and J. Sapirstein, Phys. Rev. A **54**, 2714 (1996).

[22] T. Beier, G. Plunien, M. Greiner, and G. Soff, J. Phys. B **30**, 2761 (1997).

[23] G. Plunien, T. Beier, G. Soff, and H. Persson, Eur. Phys. J. D **1**, 177 (1998).

[24] A. Mitrushenkov, L. Labzowsky, I. Lindgren, H. Persson, and S. Salomonson, Phys. Lett. A **200**, 51 (1995).

[25] S. Mallampalli and J. Sapirstein, Phys. Rev. A **57**, 1548 (1998).

[26] V. A. Yerokhin and V. M. Shabaev, Phys. Rev. A **64**, 062507 (2001).

[27] V. A. Yerokhin, P. Indelicato, and V. M. Shabaev, Phys. Rev. Lett. **91**, 073001 (2003).

[28] V. A. Yerokhin, P. Indelicato, and V. M. Shabaev, Eur. Phys. J. D **25**, 203 (2003).

[29] V. A. Yerokhin, P. Indelicato, and V. M. Shabaev, Phys. Rev. A **71**, 040101(R) (2005).

[30] V. A. Yerokhin, P. Indelicato, and V. M. Shabaev, Zh. Eksp. Teor. Fiz. **128**, 322 (2005) [JETP **101**, 280 (2005)].

[31] V. A. Yerokhin, P. Indelicato, and V. M. Shabaev, Phys. Rev. Lett. **97**, 253004 (2006).

[32] N. J. Snyderman, Ann. Phys. (NY) **211**, 43 (1991).

[33] V. A. Yerokhin and V. M. Shabaev, Phys. Rev. A **60**, 800 (1999).

[34] V. A. Yerokhin, K. Pachucki, and V. M. Shabaev, Phys. Rev. A **72**, 042502 (2005).

[35] P. Indelicato and P. J. Mohr, Phys. Rev. A **46**, 172 (1992).

[36] P. J. Mohr, G. Plunien, and G. Soff, Phys. Rep. **293**, 227 (1998).

[37] M. Gyulassy, Nucl. Phys. A **244**, 497 (1975).

[38] G. Soff and P. J. Mohr, Phys. Rev. A **38**, 5066 (1988).

[39] A. N. Artemyev, V. M. Shabaev, and V. A. Yerokhin, Phys. Rev. A **56**, 3529 (1997).

[40] A. G. Fainshtein, N. L. Manakov, and A. A. Nekipelov, J. Phys. B **24**, 559 (1991).

[41] P. Indelicato and P. J. Mohr, Theor. Chim. Acta **80**, 207 (1991).

[42] S. A. Blundell, K. T. Cheng, and J. Sapirstein, Phys. Rev. A **55**, 1857 (1997).

[43] H. Persson, S. Salomonson, P. Sunnergren, and I. Lindgren, Phys. Rev. A **56**, R2499 (1997).

[44] P. Indelicato and P. J. Mohr, Phys. Rev. A **63**, 052507 (2001).

[45] V. A. Yerokhin, A. N. Artemyev, V. M. Shabaev, and G. Plunien, Phys. Rev. A **72**, 052510 (2005).

[46] I. Angeli, At. Data Nucl. Data Tables **87**, 185 (2004).

[47] Y. S. Kozhedub, O. V. Andreev, V. M. Shabaev, I. I. Tupitsyn, C. Brandau, C. Kozhuharov, G. Plunien, and T. Stöhlker, Phys. Rev. A **77**, 032501 (2008).

[48] W. R. Johnson and G. Soff, At. Data Nucl. Data Tables **33**, 405 (1985).

[49] K. Pachucki, Phys. Rev. A **48**, 2609 (1993).

[50] M. I. Eides and H. Grotch, Phys. Lett. B **301**, 127 (1993).

[51] S. G. Karshenboim, Zh. Eksp. Teor. Fiz. **109**, 752 (1996) [JETP **82**, 403 (1996)].

[52] U. D. Jentschura, A. Czarnecki, and K. Pachucki, Phys. Rev. A **72**, 062102 (2005).

[53] V. M. Shabaev, I. I. Tupitsyn, V. A. Yerokhin, G. Plunien, and G. Soff, Phys. Rev. Lett. **93**, 130405 (2004).

[54] M. I. Eides, H. Grotch, and D. Owen, Phys. Lett. B **294**, 115 (1992).

[55] G. Källen and A. Sabry, Mat. Fys. Medd. K. Dan. Vidensk. Selsk. **29**, 17 (1955).

[56] J. Schwinger, *Particles, sources, and fields* (Reading, Mass, Addison-Wesley, 1973).

[57] M. Barbieri and E. Remiddi, Nuovo Cimento **13**, 99 (1973).

[58] D. Broadhurst, J. Fleischer, and O. Tarasov, Z. Phys. C **60**, 287 (1993).

[59] L. W. Fullerton and J. G. A. Rinker, Phys. Rev. A **13**, 1283 (1976).

[60] T. Appelquist and S. J. Brodsky, Phys. Rev. A **2**, 2293 (1970).

[61] A. I. Milstein, O. P. Sushkov, and I. S. Terekhov, Phys. Rev. Lett. **89**, 283003 (2002).

[62] A. I. Milstein, O. P. Sushkov, and I. S. Terekhov, Phys. Rev. A **69**, 022114 (2004).

[63] M. Baranger, F. Dyson, and E. Salpeter, Phys. Rev. **88**, 680 (1952).

[64] M. I. Eides and V. A. Shelyuto, Phys. Rev. A **52**, 954 (1995).

[65] G. S. Adkins and Y. Zhang, Can. J. Phys. **76**, 333 (1998).